

1 CdSe nanowires with illumination-enhanced conductivity: Induced dipoles, 2 dielectrophoretic assembly, and field-sensitive emission

3 Ronghui Zhou and Hsueh-Chia Chang^{a),b)}

4 *Department of Chemical and Biomolecular Engineering, University of Notre Dame,*
5 *Notre Dame, Indiana 46556*

6 Vladimir Protasenko and Masaru Kuno^{a),c)}

7 *Department of Chemistry and Biochemistry, University of Notre Dame, Notre Dame, Indiana 46556*

8 Amol Kumar Singh, Debdeep Jena, and Huili (Grace) Xing^{a),d)}

9 *Department of Electrical Engineering, University of Notre Dame, Notre Dame, Indiana 46556*

10 (Received 18 September 2006; accepted 24 January 2007)

11 Positive ac dielectrophoresis (DEP) is used to rapidly align ensembles of CdSe semiconductor
12 nanowires (NWs) near patterned microelectrodes. Due to their large geometric aspect ratio, the
13 induced dipole of the wires is proportional to their conductivity, which can be drastically enhanced
14 under super-band-gap illumination by several orders of magnitude, with a corresponding increase in
15 the wire DEP mobility. This optical enhancement of conductivity occurs because of the generation
16 of mobile electrons and holes and is verified by a photocurrent measurement. The linear nanowire
17 alignment exhibits a high degree of fluorescent polarization anisotropy in both absorption and
18 emission. An unexpected observation is a reversible, factor of ~ 4 , electric-field-induced, and
19 frequency-dependent enhancement of the nanowire emission near 10 Hz. Such
20 illumination-sensitive, field-enhanced, and frequency-dependent alignment and emission
21 phenomena of NWs suggest an electrical-optical platform for fabricating CdSe nanowire devices for
22 polarization-sensitive photodetection and biosensing applications. © 2007 American Institute of
23 *Physics*. [DOI: 10.1063/1.2714670]

25 INTRODUCTION

26 A great deal of research in nanostructures (nanocrystals
27 and nanowires) has focused on demonstrating that these ma-
28 terials can be employed in devices such as field-effect tran-
29 sistors, photodetectors, and light-emitting diodes, in a man-
30 ner akin to uses of conventional bulk solids.¹ At the same
31 time, solution-based semiconductor nanostructures such as
32 CdSe nanowire^{2,3} (NW) colloidal quantum dots (QDs) [or
33 nanocrystals (NCs)]⁴ offer added degrees of freedom, distinct
34 from bulk behavior. In principle, these properties can be ex-
35 ploited and thus represent a paradigm shift for device appli-
36 cations. For example, nanostructures suspended in a dielec-
37 tric medium can be reversibly moved in and out of solution
38 using external stimuli,⁵ forming conductive as well as opti-
39 cally active networks in precisely defined regions of a
40 substrate.⁶ This controllable self-assembly, coupled to size-
41 dependent optical and electrical properties,² opens up pow-
42 erful fabrication techniques for nanostructure-based devices.

AQ: #1
43 Among low dimensional materials, semiconductor NWs
44 exhibit strong photoconductivity,^{7,8} as well as visible
45 fluorescence,^{9,10} due to their direct band gap nature. They do
46 not suffer from problems associated with admixtures of me-
47 tallic and semiconducting species, commonly encountered in
48 carbon nanotubes (CNTs).¹¹ Furthermore, they can be made
49 to emit in the visible by suitably modifying the size and

shape of the nanostructure.¹² These dependencies have been **50**
theoretically modeled for quasi-one-dimensional systems **51**
such as semiconductor nanorods (NRs).¹³ **52**

Because CdSe NWs have the same crystal structure as **53**
corresponding NRs and QDs, albeit with larger aspect ratios, **54**
they have similar optical properties. However, significant dif- **55**
ferences between NWs and NRs (or NCs) exist, including the **56**
presence of one-dimensional (1D) excitons,^{14,15} potential di- **57**
electric contrast effects,^{14,15} enhanced 1D exciton binding **58**
energies,¹⁵ variations in the effective fluorescence quantum **59**
yield, and strong changes in the density of states underlying **60**
the linear absorption. An additional difference, important for **61**
field-directed nanocircuit assembly but seldom noted, is the **62**
fact that NWs possess potentially significant induced and/or **63**
permanent dipole moments due to their highly anisotropic **64**
shapes. In this respect, NW aspect ratios can reach values of **65**
 10^3 or more due to their narrow diameters (< 10 nm) and **66**
micron long lengths.^{2,3} When coupled to the presence of a **67**
polar wurtzite (WZ) phase, CdSe NWs, grown along the *c* **68**
axis ($\langle 0001 \rangle$ direction), can therefore behave as giant elec- **69**
trets in the absence of an external electric field. More spe- **70**
cifically, hexagonal CdSe possesses a spontaneous polariza- **71**
tion on the order of $P \sim 0.2 - 0.6 \mu\text{C}/\text{cm}^2$. [Actual literature **72**
estimates are $P = 0.19$,¹⁶ $P = 0.42$,¹⁷ and $P = 0.6 \mu\text{C}/\text{cm}^2$ (Ref. **73**
18).] These numbers are comparable to some of the largest **74**
values seen in wurtzite III-V semiconductors such as GaN **75**
($\sim 3 \mu\text{C}/\text{cm}^2$).¹⁹ Even in CdSe NWs with admixtures of **76**
wurtzite and zinc blende (ZB) as well as twinned ZB **77**

^{a)}Authors to whom correspondence should be addressed.

^{b)}Electronic mail: hchang@nd.edu

^{c)}Electronic mail: mkuno@nd.edu

^{d)}Electronic mail: hxing@nd.edu

78 sections,³ many smaller dipoles might exist within individual
79 wurtzite links (all aligned end to end along the NW length),
80 giving rise to a significant permanent dipole.

81 Assembly of nanocircuitry involving NWs requires a
82 mechanism to manipulate and assemble the NWs—a force
83 must be imparted on the NWs to direct their assembly into
84 functional circuits. The permanent dipoles offer such a
85 mechanism by generating an electric torque on the NW in an
86 applied field that can align them along the field line. The
87 aligned NWs would not experience a net force in a spatially
88 uniform field but will suffer one in a nonuniform dc field.
89 For NWs, the resulting mobility is in the direction of the
90 high field region, known as positive dc dielectrophoresis
91 (DEP). In a nonuniform ac field, on the other hand, there
92 would be no force on the aligned permanent dipoles.

93 Other than permanent dipoles, NWs are also endowed
94 with a large polarizability such that they exhibit high induced
95 dipoles in an electric field. For NWs and CNTs that are more
96 conducting than the medium, induced ac dipoles are parallel
97 to the field. As they reverse polarity with the ac field, a
98 spatially nonuniform ac field can impart a net (time-
99 averaged) Maxwell force on the NWs and CNTs such that
100 they exhibit a net motion in the direction of the higher field
101 (positive DEP). This ac dielectrophoresis phenomenon is
102 preferred over dc dielectrophoresis of permanent dipoles (or
103 dc induced dipoles), as high frequency ac fields do not carry
104 a net current and hence do not produce undesirable Faradic
105 products such as bubbles and contaminating ions during the
106 assembly.²⁴

AQ: #2 107 The permanent and induced dipoles could further pro-
108 duce dipolar or induced-dipolar interaction to assemble the
109 NW into aligned structures. A promising nanocircuitry fabri-
110 cation technique is hence to sort and manipulate NWs and
111 CNTs dielectrophoretically with sequentially activated local
112 fields, sustained by micro-fabricated ac microelectrodes or
113 microchannels, such that the NWs assemble into complex
114 nanonetworks of field-effect transistors, photoemitters, and
115 sensors. Although a functional nanocircuitry has yet to be
116 assembled in this manner, simple array assembly has been
117 demonstrated in the alignment of metal NWs by
118 dielectrophoresis.²⁰ The approach thus complements other
119 potential fabrication techniques for nanowires, including
120 Langmuir-Blodgett^{21–23} and microfluidic alignment.^{24,25}

121 There are more reports of CNT assembly and alignment by
122 DEP,^{24–28} although the application of CNTs is still severely
123 limited by their nonuniform band gap in the mixture (i.e.,
124 metallic versus semiconducting tubes with a range of band
125 gap).

126 Unlike spherical nanocolloids whose DEP mobility is in-
127 sensitive to particle/medium conductivity, the large NW as-
128 pect ratio also endows NWs with a DEP mobility that is
129 proportional to the NW conductivity. This is particularly per-
130 tinent in the present study, as we shall demonstrate that, un-
131 der super-band-gap illumination, charge carriers can be gen-
132 erated in the CdSe NWs such that its conductivity can
133 increase by orders of magnitude. Thus, their DEP mobility is
134 greatly enhanced. Moreover, we shall demonstrate that the
135 same illumination-generated carriers can enhance bundling
136 of NWs, which has profound implications in sensing appli-

cations. For example, ensembles of aligned NWs have been
used to promote the capture of pathogens such as bacteria²⁴
both at the ensemble and single particle levels. In this re-
spect, the illumination-enhanced field at the end of the NW
can promote pathogen-NW dipole-induced “docking” as sup-
ported by our earlier work on the DEP trapping of CNTs and
CNT/bacteria mixtures.²⁴ Underlying this phenomenon is an
induced dipole-induced dipole attraction with an interaction
potential energy of ~ 50 kT as calculated from their dielec-
trophoretic velocity. Furthermore, given the direct band gap
emission of the wires, changes in their emission intensity
after pathogen docking may provide an alternative means of
sensing apart from standard conductivity measurements.¹
The illumination-enhanced assembly of NW under an ap-
plied ac electric field, their fluorescence behavior both in the
presence and absence of the field as well as their correspond-
ing transport properties are therefore of practical interest for
aforementioned potential applications.²⁹

154 AQ: #3
155 These interesting electric-optical properties of CdSe
156 NWs during and after assembly suggest a potentially power-
157 ful electrical-optical fabrication platform for sensing nanocir-
158 cuitries based on CdSe NWs. Our investigation of this ap-
159 proach involves visual confirmation of NW alignment with
160 subsequent bright field and epifluorescence measurements.
161 The ac dielectrophoretic velocity of semiconducting NWs is
162 shown to be enhanced using super-band-gap illumination by
163 three orders of magnitude higher than that due to pure dielec-
164 tric polarization and migration of intrinsic charge carriers on
165 the NW, depending on the illumination intensity. As ex-
166 pected, a corresponding increase in DEP mobility and assem-
167 bly speed is observed. These rapidly aligned assemblies ex-
168 hibit strong polarization anisotropies in both the absorption
169 and emission. As previously emphasized, an unexpected en-
170 hancement of the NW emission, by a factor of ~ 4 , is ob-
171 served in the presence of an electric field. This behavior is
172 unexpected as such a field is generally anticipated to quench
173 any emission due to the reduced spatial overlap between
174 electron and hole wave functions,³⁰ though it is possible that
175 enhanced 1D exciton binding energies could suppress this
176 effect.¹⁵ AQ: #4

EXPERIMENTS 177

178 Narrow diameter (< 10 nm) CdSe NWs with lengths be-
179 tween 1 and 10 μm were synthesized using a seeded solution
180 approach.^{2,3} The asymmetric growth is catalyzed in the pres-
181 ence of mild coordinating surfactants such as trioctylphos-
182 phine oxide (TOPO), using low melting, bimetallic Au/Bi
183 core/shell nanoparticles (NPs). Such bimetallic Au/Bi cata-
184 lysts have also been used in the solution phase synthesis of
185 other NWs including PbSe (Ref. 31) and more recently
186 CdTe.³² As a representative low resolution transmission elec-
187 tron microscope (TEM) micrograph shown in Fig. 1(a), these
188 CdSe NWs have diameters between 7 and 10 nm and lengths
189 exceed 1 μm (> 10 μm in some cases). Corresponding di-
190 ameter distributions are on the order of 25%. Figure 1(b)
191 shows that the wires are crystalline and uniform, with in-
192 trawire diameter distributions between 3% and 6%.^{3,9} Al-
193 though the high resolution micrograph in Fig. 1(b) shows

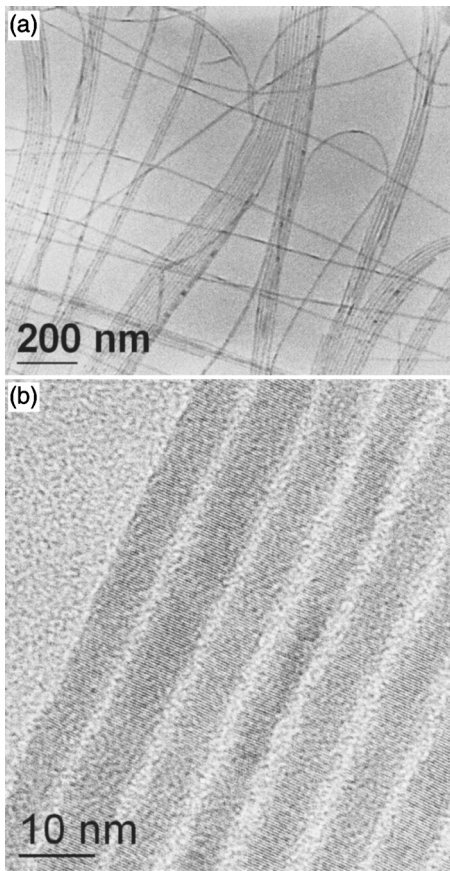


FIG. 1. (a) Low and (b) high resolution TEM images of CdSe NWs.

were generated using a function generator connected to a high voltage amplifier. Corresponding ac frequencies were varied between 0.2 Hz and 10 MHz.

Fluorescence measurements, both during and after NW alignment and both in the chloroform solvent and in air, were carried out using a modified, single molecule sensitive, inverted optical microscope. The excitation source is the 488 nm line of an air cooled Ar⁺ ion laser, filtered to remove any residual plasma light. The light is then passed through a polarization preserving single mode fiber to ensure a Gaussian TEM₀₀ mode. It is then recollimated with a microscope objective, effectively expanding the beam's waist to ~8 mm. The orientation of the light's linear polarization is controlled using a half wave plate mounted on a rotation stage. A quarter wave plate is subsequently inserted after the $\lambda/2$ plate to create circularly polarized light for subsequent emission polarization anisotropy experiments. These experiments also involve placing an additional linear polarizer (analyzer) prior to the detector.

The microscope can be operated confocally by overfilling the back aperture of the 1.4 numerical aperture (NA) oil immersion objectives with collimated light. Alternatively, for epiillumination, an $f=250$ mm lens is inserted to focus the light prior to the objective's back aperture. This creates a wider excitation area on the sample, with a field of view reaching 30 μm in diameter. Typical excitation intensities used in our experiments range from 1 to 100 W/cm². Emitted light from the sample is collected with the same objective and is passed through two barrier filters to remove any excess excitation light. The emission is then imaged using either a single photon counting avalanche photodiode (Perkin Elmer SPCM AQR-14) or with a Peltier cooled charge-coupled device (CCD) (DVC 1412). More information about the apparatus can be found in Ref. 9.

Transport properties of aligned nanowires were studied through I - V measurements taken on an Agilent 4155B semiconductor parameter analyzer. The applied bias ranged from -40 to 40 V with obtained currents in the range of 1 pA-1 μA . Samples for these measurements were prepared by first aligning the wires between the interdigitated electrodes and letting the solvent dry with the field on. Some samples were also processed via rapid thermal annealing in order to improve the contact between the wires and the electrodes. All measurements were conducted under ambient conditions.

RESULTS AND DISCUSSIONS

In general, a number of ways exist for manipulating nanoscale objects using ac or dc electric fields.³³ For example, charged particles (or nanostructures) in solution can directly undergo electrophoresis in the presence of a uniform dc field. By contrast, nanostructures with a permanent dipole moment simply orient along the field lines due to the equal but opposing forces pulling on either side of the dipole. On the other hand, a nonuniform field can be used to manipulate neutral particles with induced and/or permanent dipoles, i.e., dielectrophoresis. In dc DEP, both permanent and induced dipoles contribute to the motion of the particle; in symmetric

that the wires are crystalline, it hides the fact that individual NWs exhibit admixtures of zinc blende and wurtzite phases. This can be seen in properly oriented ($\langle 110 \rangle$ zone) wires, as described in more detail in Ref. 3. Nanowires with branched morphologies can also be made using variations of the approach, involving different initial metal to chalcogen precursor ratios.³ In all cases, NW surfaces are passivated with organic ligands such as trioctylphosphine oxide, trioctylphosphine, and octanoic acid. As a consequence, the recovered NWs can be resuspended in common organic solvents such as toluene or chloroform. All our experiments are performed with a chloroform solvent. Despite the solvent's low molecular weight, we observed little sedimentation or bundling since the DEP field is activated before sedimentation occurs and the organic ligands on the surface of the wires provide steric stabilization. These CdSe NWs have an absorption edge at ~1.8 eV (in comparison, the band gap of bulk CdSe is 1.78 eV).

The gold microelectrodes employed in this study were patterned using standard photolithography and lift-off process. Specifically, masks were used to define interdigitated electrodes with a 20-40 μm gap, and then 5 nm of titanium was sputtered onto a microscope coverslip as an adhesion layer for the subsequent evaporation of 45 nm of Au. A piece of cover well was glued above the electrodes to create an ~100 μl perfusion chamber. This prevented samples from drying too quickly during NW alignment experiments. ac electric fields with magnitudes ranging from 1 to 40 kV/cm

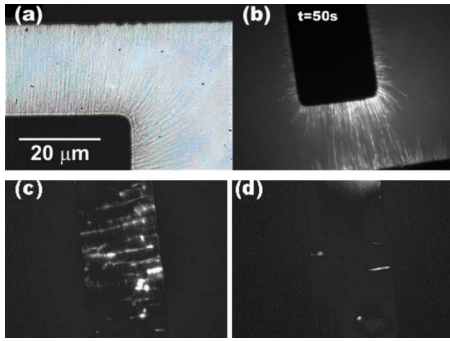


FIG. 2. Dielectrophoretically aligned CdSe NWs using an ac electric field (10 V) with electrodes separated by a 20 μm gap. [(a) and (b)] (1 MHz) Resulting bright field image after alignment and epifluorescence image taken at $t=50$ s during the alignment, respectively. [(c) and (d)] (10 kHz) Resulting alignment in 190 s, under illumination (~ 100 W/cm 2 at 488 nm) and in dark, respectively.

aligned NWs and their surrounding medium can be modeled as capacitors (dielectrics) and resistors (conductors) in parallel. Dielectric polarization occurs at high frequencies when atomic dipoles form within the NW. As opposing charges of two nearby atomic dipoles cancel each other, there is no net charge within the NW at a coarsened mesoscale. A net interfacial charge exists, however, at the NW interface due to the different dielectric constants (and atomic dipole intensity) of the two media surrounding the interface. As the interfacial normal field is highest at the two ends of the NW, two localized charges of opposite sign result at the two ends to produce a dielectrically induced NW dipole. At lower frequencies, when current-carrying space charges have sufficient time to migrate to and accumulate at the two ends (if the medium conductivity is lower), a conductive polarization mechanism begins to dominate the induced dipole formation process. Hence, differences in conductivity and dielectric constant of the NW relative to its surrounding medium enable the creation of induced charges at either end of the wire in the presence of an electric field. A key ingredient of the low frequency conductive mechanism is that it requires a conducting NW with mobile charge carriers. The magnitude of the aligned induced dipole by either mechanism can be calculated using

$$\mu_{\text{ind}}(t) = \epsilon_0 \epsilon_m V_{\text{NW}} K E(t), \quad (1)$$

where ϵ_m is the relative dielectric constant of the medium, ϵ_0 is the vacuum permittivity, and V_{NW} is the NW volume. K is the complex Clausius-Mossotti factor, which depends on the complex dielectric constant of the NW and that of the surrounding medium and captures both dielectric and conductive effects. Simplifying the above expression is the significantly larger longitudinal polarizability of a NW relative to its transverse (radial) polarizability. As a consequence, K for a nanowire with a corresponding Lorentz depolarization factor of $n \sim 0$ (Ref. 30) can be approximated by

$$K = \frac{(\epsilon_{\text{NW}}^* - \epsilon_m^*)}{\epsilon_m^*}. \quad (2a)$$

The complex dielectric constant $\epsilon_{\text{NW}(m)}^* = \epsilon_{\text{NW}(m)} \epsilon_0 - i \sigma_{\text{NW}(m)} / \omega$ of both the NW and its surrounding medium is expressed in terms of their respective conductivities, $\sigma_{\text{NW}(m)}$, as well as the angular frequency of the applied field, ω . In contrast, the complex Clausius-Mossotti factor for a sphere is

$$K = \frac{\epsilon_p^* - \epsilon_m^*}{\epsilon_p^* + 2\epsilon_m^*}, \quad (2b)$$

and $|K| \leq 1$ for all medium/particle conductivities and permittivities. As such, for high conductivity and high permittivity nanocolloids, K approaches unity at both high and low frequency limits. There is hence little sensitivity to particle conductivity or permittivity for spherical nanocolloids. The effective polarizability of NWs with larger aspect ratio, on the other hand, can be much higher than unity if either conductivity or permittivity is much higher than that of the medium.

ac DEP, only induced dipoles contribute to the motion of the particle.²⁵ Specifically, when a highly polarizable, but uncharged, object such as a nanowire is subjected to an electric field, an induced dipole moment is created, enabling the object to respond to electric field gradients that are present.

In our experiments, the NWs dispersed in chloroform were observed to quickly assemble under microscope illumination between the electrodes under a reasonably strong ac electric field (>1 kV/cm) at all frequencies investigated. The alignment was detected visually through both bright field and epifluorescence measurements. Shown in Fig. 2 are aligned NWs spanning a 20 μm electrode pair. The applied ac signal had a peak voltage of 10 V, corresponding to $E_{\text{rms}} = 3.5$ kV/cm. Figure 2(a) is a bright field image. Apparently, the aligned NWs follow the electric field lines. Figure 2(b) shows the epifluorescence image of the same alignment under microscope illumination at $t=50$ s after the field is activated. NW assembly occurs at both electrodes as expected for a particle experiencing a positive DEP force. To illustrate the effect of super-band-gap illumination, epifluorescence images of aligned NWs were captured both under 488 nm illumination and in dark, shown in Figs. 2(c) and 2(d), respectively. It is evident that the assembly speed of CdSe NWs is much faster under illumination. In the chloroform medium ($\eta=0.58$ cP), the estimated DEP velocity is 100 $\mu\text{m}/\text{s}$ under illumination compared to less than 1 $\mu\text{m}/\text{s}$ in dark. These indicate that the DEP force and velocity of the NW have a strong dependence of its conductivity.

The dielectrophoretic behavior of NWs can be treated within the context of a Maxwell-Wagner formalism. If the NW and its induced dipole are not aligned with the local field, it suffers a net torque even in a spatially uniform ac field, even though there is no net translational DEP motion. As such, the rotational velocity is higher than the translational velocity by a factor that is equal to the aspect ratio of the NW, as the field gradient necessary to produce DEP translation has a length scale corresponding to the length of the NW while the dipole intensity is determined by a cross section of the NW. There is hence a rapid alignment with the field, and the subsequent DEP motion of the NW corresponds to the one that is aligned with the local field. Both the

AQ: #5

AQ: #6

371 The time-averaged dielectrophoretic force on the wire,
372 due to the interaction between its dipole moment and the
373 electric field gradient, can be expressed by³⁰

$$374 \quad F_{\text{DEP}} = \mu(t) \cdot \nabla E(t) = \frac{1}{2} (\pi r^2 L) \epsilon_m \text{Re}\{K\} \nabla |E_{\text{rms}}|^2, \quad (3)$$

375 where E_{rms} is the root mean square value of the electric field
376 and the cylinder volume is calculated using its radius r and
377 length L . The direction of DEP motion depends on the sign
378 of the real part of the Clausius-Mossotti factor K . This pa-
379 rameter captures the field-induced dielectric polarization of
380 NW and medium atoms or molecules as well as that due to
381 capacitive charging currents within both the NW and the
382 medium.³⁴ Depending on the orientation of the dipole rela-
383 tive to the ac electric field as well as the permittivity and
384 conductivity of the NW/medium, the wire can move towards
385 either the high (positive DEP) or low (negative DEP) field
386 region. The dielectrophoretic velocity of the NW is obtained
387 by equating the DEP force to the viscous drag of the NW and
388 scales as the DEP force of (3) divided by the NW length L
389 and the medium viscosity. The DEP mobility is the factor in
390 front of the gradient of the squared field intensity in the DEP
391 velocity and is proportional to the real part of the Clausius-
392 Mossotti factor K .

393 Equations (4) and (5) show both the high and low fre-
394 quency limits of the real part of K ,

$$395 \quad \text{Re}\{K\} = \frac{(\epsilon_{\text{NW}} - \epsilon_m)}{\epsilon_m} \quad (\omega \rightarrow \infty), \quad (4)$$

$$396 \quad \text{Re}\{K\} = \frac{(\sigma_{\text{NW}} - \sigma_m)}{\sigma_m} \quad (\omega \rightarrow 0), \quad (5)$$

397 and explain why CdSe NWs in chloroform maintain a posi-
398 tive DEP force at all frequencies investigated. Namely, CdSe
399 has substantial dielectric constants, $\epsilon_{\text{NW}}=10.2$ ($\epsilon_{\perp}=9.33$,
400 transverse direction),^{16,35} and conductivities (σ_{NW}
401 $\sim 100 \mu\text{S}/\text{cm}$ measured for a single NW in dark)⁷ relative to
402 its surrounding medium. By contrast, chloroform has a rela-
403 tive dielectric constant of $\epsilon_m=4.8$ and a corresponding con-
404 ductivity of $\sigma_m=0.02 \mu\text{S}/\text{cm}$. As a consequence, K is posi-
405 tive for all frequencies considered and accounts for why
406 CdSe wires always move towards, not away from, the elec-
407 trodes. It is also apparent that all nanocolloids have small
408 DEP mobility because they cannot overcome their small vol-
409 ume factor $4/3\pi r^3$ for spheres in (3) by increasing its con-
410 ductivity. In contrast, NWs can overcome this short dipole
411 length limitation by increasing their conductivity as shown in
412 (2a). As a result, conducting NWs have much higher DEP
413 mobility than conducting spherical nanocolloids of the same
414 volume. As seen in the NW transport properties described
415 later in this paper, the conductivity of the NW can be easily
416 enhanced by orders of magnitude even with moderate illumi-
417 nation intensity and we hence expect a corresponding in-
418 crease in DEP mobility.

419 A positive DEP force is also observed at 10 MHz unlike
420 common bioparticles, which transition from positive to nega-
421 tive DEP forces occurs at an ac crossover frequency between
422 100 kHz and 1 MHz.^{24,33,36} That positive DEP occurs only at

a relative low frequency is a problem for DEP-based sensors 423
since the low crossover frequency makes the DEP trapping 424
field short ranged due to double layer screening at the 425
electrode²⁴ and the possibility of Faradaic reaction at the 426
electrodes. By contrast, the 10 MHz positive DEP force seen 427
in NWs enables the field to penetrate further into the sur- 428
rounding medium. It also allows a means of separating bac- 429
teria captured by NW and those that have not docked with 430
NW in our earlier strategy of using the high induced dipoles 431
of nanostructures to capture pathogens.³⁰ 432

In aligned NW ensembles, we observe long-chain linear 433
NW bundles due to dipole-dipole (end-to-end) interactions 434
between either induced or permanent dipoles. Although per- 435
manent dipoles do not contribute to ac dielectrophoresis, 436
they can still be responsible for the assembly. Our assembly 437
structure is similar to those formed by single wall nanotubes 438
(SWNTs) assembled from organic solutions.^{37,38} Based on 439
simple dipole-dipole interaction considerations, $U(r)$ 440
 $= -\mu_1\mu_2/2\pi\epsilon_m\epsilon_0 r^3$, we obtain an estimated interaction po- 441
tential energy between two side-to-side oriented 50 D wurtz- 442
ite NW sections of $\sim 0.5 \text{ eV}$ ($\sim 20 \text{ kT}$). This assumes an in- 443
terwire spacing of 1.1 nm based on the presence of TOPO 444
ligands on NW surfaces.³⁹ We have also estimated that a 445
10 nm diameter wurtzite CdSe NW possesses an intrinsic 446
permanent dipole moment, due to spontaneous polarization, 447
of roughly 50L D, where L is the length of the nanowire 448
expressed in nanometers. Based on conservative estimates of 449
the spontaneous polarization for CdSe, $P \sim 0.2 \mu\text{C}/\text{cm}^2$, a 450
10 nm diameter wire has a total surface charge density of 451
 $\sigma_o = 1.25 \times 10^{12} \text{ e}/\text{cm}^2$. The product of this and the surface 452
area normal to the wire growth axis gives ~ 1 electron per 453
NW end face. The corresponding permanent dipole moment 454
is then $\mu = (1.602 \times 10^{-19} \text{ C})(1 \times 10^{-9} \text{ m}/\text{nm})(L)/3.336$ 455
 $\times 10^{-30} \text{ C m/D}$ or 48L D for a pristine 10 nm diameter 456
wurtzite CdSe NW, grown along the $\langle 0001 \rangle$ direction in 457
vacuum. In the presence of mobile carriers generated by pho- 458
tons in the NW, a charge density will be established at either 459
end of the nanowire during each half cycle of the ac field. To 460
illustrate, each charge localized at the end of the wire causes 461
a 50 000 D dipole moment in a 1 μm long NW. Therefore, a 462
much larger interaction potential energy between NWs will 463
result under super-band-gap illumination. Such large interac- 464
tion potential energies would, in turn, suggest induced 465
dipole-dipole interactions as the root cause of “bundling” 466
commonly seen in NW ensembles,^{2,3} which can be drasti- 467
cally enhanced by photon-generated charge carriers. 468

Additional characterization of aligned NW ensembles in 469
air, after chloroform has evaporated, was conducted through 470
absorption and emission polarization anisotropy measure- 471
ments. In these experiments, a 1 kHz ac electric field (E_{rms} 472
 $= 5 \text{ kV}/\text{cm}$) was first used to align the NWs, fixing their 473
orientation by drying out the solution while keeping the field 474
on. Figure 3 illustrates an example of NWs oriented between 475
two electrodes. The linear polarization of the excitation was 476
subsequently rotated using a $\lambda/2$ wave plate. Epifluores- 477
cence images of the ensemble [Figs. 3(a) and 3(b)] clearly 478
show changes in the emission intensity with polarization 479
angle. A movie illustrating this is also provided in the sup- 480
porting information section. 481

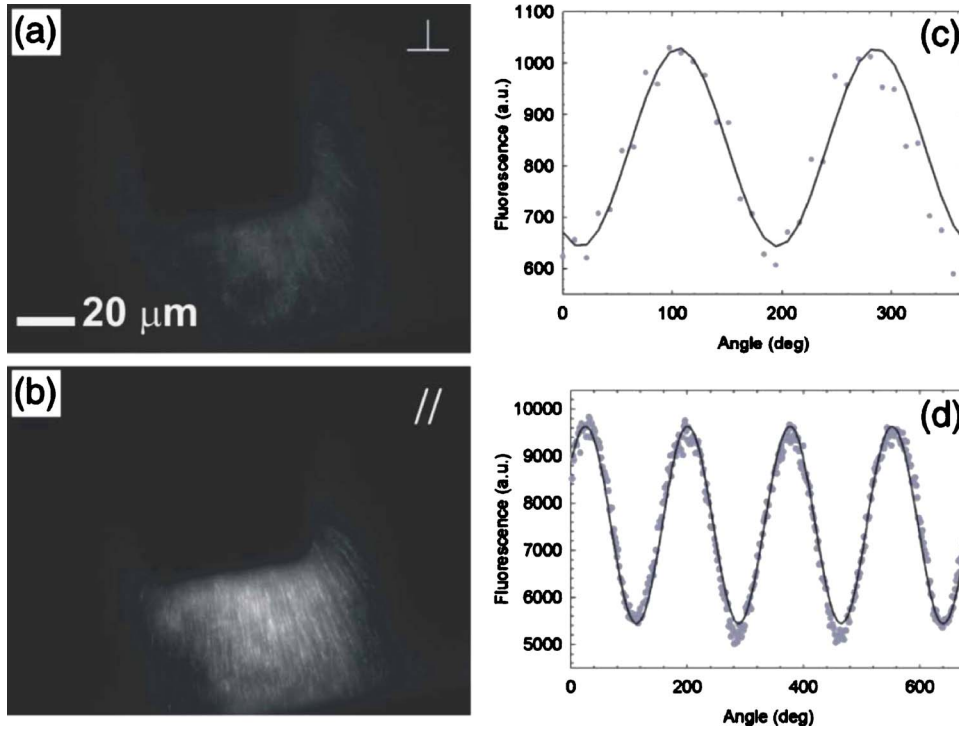


FIG. 3. (a) Fluorescence images from the absorption polarization anisotropy of aligned NW ensembles in air. (b) Corresponding plot of the absorption polarization anisotropy. (c) Plot of the emission polarization anisotropy from a different aligned ensemble.

482 Typical absorption (emission) polarization anisotropies,
 483 $\rho = (I_{\parallel} - I_{\perp}) / (I_{\parallel} + I_{\perp})$, of aligned samples [$I_{\parallel(\perp)}$ are the intensi-
 484 ties of the emitted light parallel (perpendicular) to the NW
 485 length] were determined to be $\rho \sim 0.24$ (0.27) by fitting the
 486 angle dependent intensity ratio [Figs. 3(c) and 3(d)] to a
 487 $\cos^2 \theta$ function. Values for the ensemble intensity were ob-
 488 tained by averaging intensities from seven random locations
 489 within the electrode gap. Although the results show signifi-
 490 cant net absorption/emission anisotropies, their values are
 491 suppressed relative to that seen in individual bundles as well
 492 as in individual NWs. To illustrate, rather than randomly
 493 sample the intensity in the electrode gap, if we focus only on
 494 the emission intensity from resolved bundles in the array,

values of the absorption (emission) polarization anisotropy 495
 jump to $\rho = 0.74$ ($\rho = 0.60$). This confirms our visual observa- 496
 tion that the actual NW dielectrophoretic alignment is incom- 497
 plete despite the high degree of overall alignment (Figs. 2 498
 and 3). Furthermore, these values are consistent with both 499
 the absorption and emission polarization anisotropies of 500
 single branched CdSe NWs seen in Fig. 4. Typical absorption 501
 (emission) polarization anisotropies from such individual 502
 NWs are found to be $\rho = 0.77$ ($\rho = 0.76$). 503

During our measurements an unusual observation was 504
 made. Namely, we observed that the electric field caused an 505
 apparent enhancement of the NW emission. More specifi- 506
 cally, the emission intensity of aligned NWs in air, measured 507

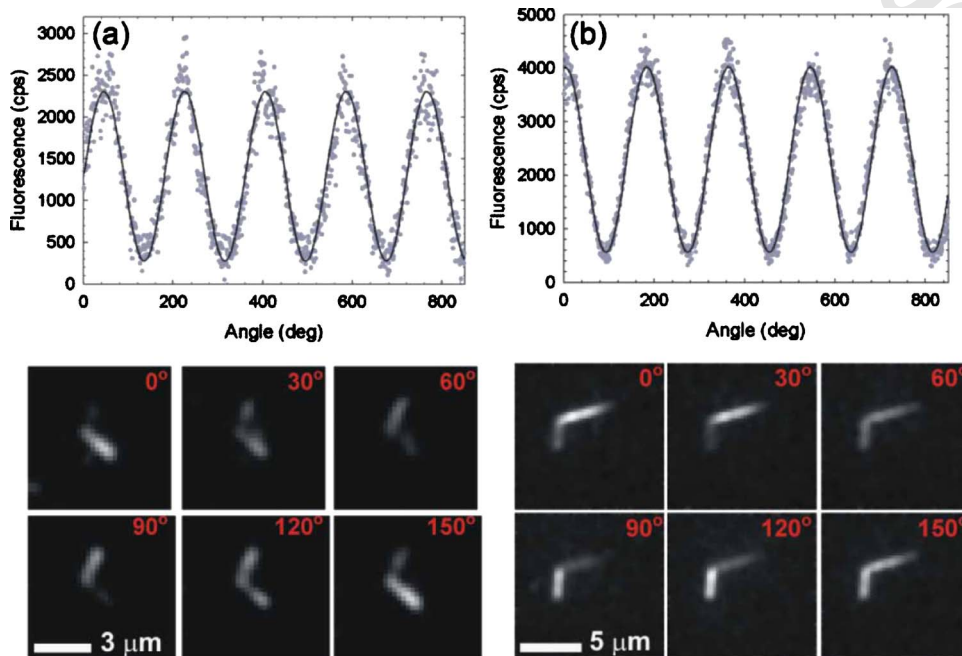


FIG. 4. (Color online) (a) Absorption and (b) emission polarization anisotropy measurements of single v-shaped CdSe NWs in air. Corresponding images of the NWs, at selected angles, are shown below.

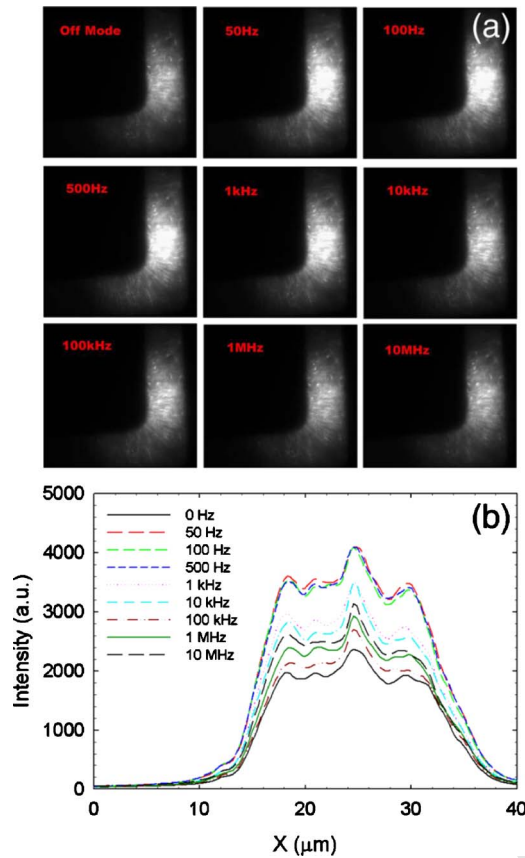


FIG. 5. (Color online) (a) Frequency-dependent fluorescence images of aligned CdSe NWs in air between 20 mm spaced electrodes. (b) Corresponding intensity cross section across the channel as a function of frequency.

508 over a range of frequencies between 0.2 Hz and 10 MHz
 509 with an ac square wave (0.5–12 kV/cm), enhances the emis-
 510 sion by a factor of ~ 4 relative to the zero field case. Figures
 511 5(a) and 5(b) show both images and an intensity cross section
 512 of aligned NWs as a function of frequency. The applied
 513 electric field is 5 kV/cm. Visual growth in the emission in-
 514 tensity is apparent, following initial increases in applied ac
 515 frequency. Higher frequencies, however, cause decreases in
 516 the enhancement, which converge to the zero field value.

517 This trend is shown more quantitatively in Fig. 6(a),
 518 which further illustrates that the same behavior is present
 519 under different electric field strengths (0.5–5 kV/cm). In all
 520 cases, a characteristic roll-off frequency of ~ 10 Hz is appar-
 521 ent, suggesting a characteristic system response time of τ
 522 ~ 100 ms. Additional characterization of the phenomenon
 523 was conducted by monitoring the emission intensity while
 524 increasing the electric field strength at a given frequency.
 525 This likewise causes fluorescence enhancements up to a fac-
 526 tor of 4. More specifically, Fig. 6(b) shows growth of the
 527 emission intensity at four fixed frequencies when field
 528 strengths are increased to 12 kV/cm. Apparent from the fig-
 529 ure is the fact that lower ac frequencies cause the largest
 530 fluorescence enhancements in contrast to higher frequencies,
 531 which suppress the effect.

532 The low frequency behavior of the emission is unex-
 533 pected as previous work on single NRs under dc electric
 534 fields has shown that externally applied fields generally act

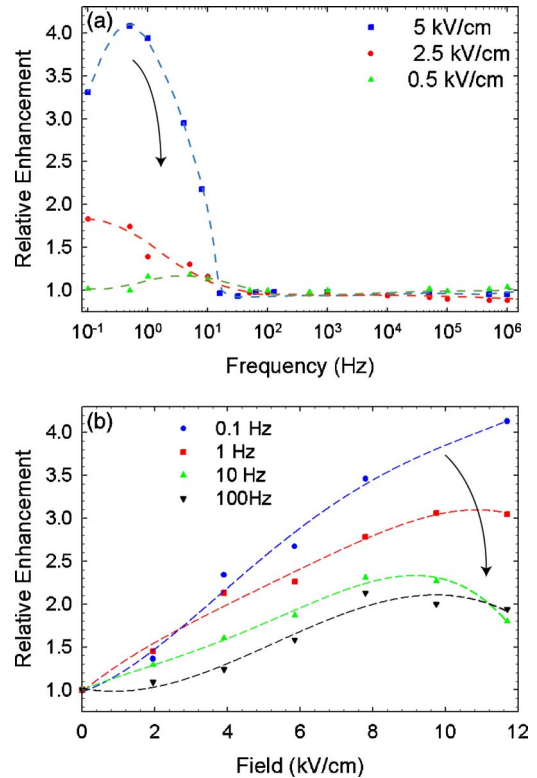


FIG. 6. (Color online) (a) Enhancements of NW emission as a function of frequency at various electric field strengths. (b) Enhancements of the NW emission as a function of electric field strength at various fixed frequencies. Dashed lines are guides to the eyes.

to reduce the electron/hole wave function overlap, causing a
 decrease of the overall emission intensity.³⁰ However, it is
 clear from the illumination-enhanced DEP discussion of (5)
 that a strong conductive current exists along the wire with a
 low frequency ac field. This same current vanishes under a
 dc field once the ends of the NW are fully charged. We hence
 speculate that this enhancement effect may be related to the
 presence of surface charges and photon-generated mobile
 carriers on or within the NW. These same charge carriers are
 responsible for the conductive currents behind illumination-
 enhanced induced dipoles and DEP mobility. The existence
 of these carriers is consistent with our recent NW FET
 measurements⁷ as well as observed blinking phenomena in
 NWs.⁴⁰ The characteristic relaxation time associated with the
 roll-off frequency could be related to the migration time of
 the carriers to one end of the NW. This charge migration is
 the charging current responsible for the field-induced polar-
 ization and dipole formation. However, a unique charge
 transport mechanism must be responsible for the long time
 scales of nearly 100 ms. Despite our incomplete understand-
 ing of the phenomenon, the unexpected ability to enhance
 the emission at low frequencies and high fields offers a po-
 tentially attractive mechanism in sensing the change of sur-
 face states, thus the substance that NWs are in contact with.

In all cases, no variations of the emission spectra were
 observed with applied electric field. This is shown in Fig. 7
 where both the field dependent emission spectra of an
 aligned ensemble and a single wire are shown together.
 While a Stark-induced redshift of the emission might be ex-

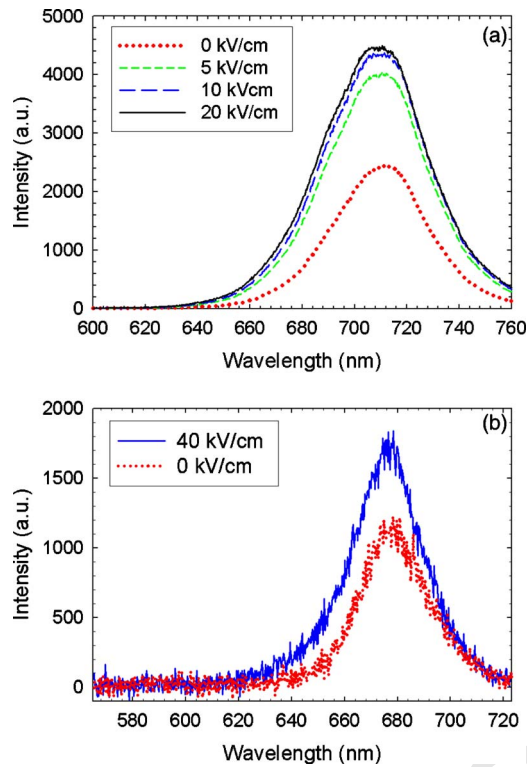


FIG. 7. (Color online) Emission spectra of (a) an aligned NW ensemble and (b) a single NW both at different electric field strengths.

pected, it is likely absent here because of the relatively low field strengths used in these experiments (0–40 kV/cm). In this respect, previous studies measuring the quantum confined Stark effect in semiconductor QDs have employed fields exceeding 100 kV/cm to reveal spectral shifts on the order of 10 meV.⁴¹ Given the low fields used in our experiments, the broad emission linewidths of both ensembles and single NWs (Ref. 9) may conceal such small Stark-induced spectral shifts, leading to no apparent change of the spectrum with electric field.

To further verify that illumination generates current carriers and changes the conductivity of the wire, the electron transport properties of aligned nanowires with and without illumination were measured using an Agilent 4155B semiconductor parameter analyzer. Prior to any thermal treatment, the as-aligned CdSe nanowires on gold contact pads exhibited non-Ohmic behavior. Currents without (with) white light illumination were <10 pA (120 pA) under an average illumination intensity of ~ 540 mW/cm² over the spectral range between 200 and 800 nm with the larger current in the presence of light indicating the strong photoconductivity of the wires.⁸ A 40 V source-drain bias was used in both cases. The low currents and non-Ohmic behavior seen in Fig. 8(a) (bottom) under optical illumination suggest poor contact between the wires and the gold electrode. This could arise from a number of reasons including the presence of surfactant on the NW surface, which acts as an insulator.

After rapid thermal annealing [1 min at 300 °C in a forming gas environment (95% N₂ 5% H₂)], however, the transport properties of the aligned wires improved markedly

AQ: #7 [Fig. 9(a), top]. Ohmic behavior was observed under optical

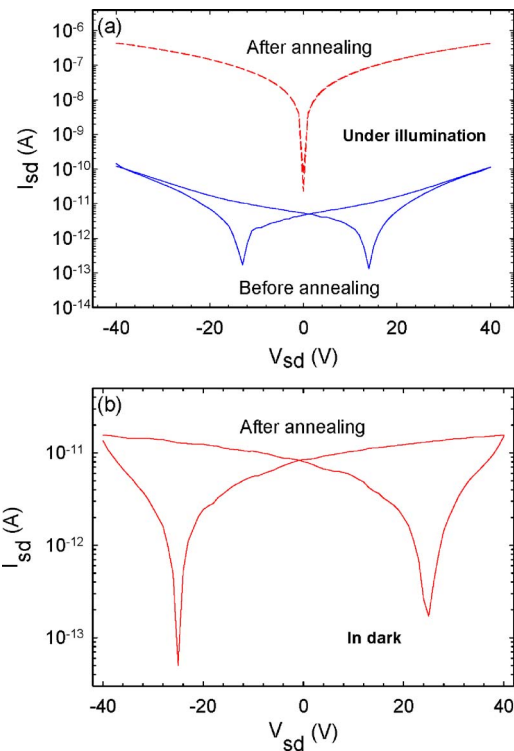


FIG. 8. (Color online) (a) Current-voltage characteristics of aligned CdSe NWs under optical illumination, both before and after rapid thermal annealing. In the latter case, a marked improvement in photocurrent is observed. (b) I - V characteristics of same device after annealing but without illumination.

illumination and currents approached 430 nA, a three order of magnitude improvement from the previous unannealed case. Even without illumination, currents of the annealed device approached 15 pA [Fig. 9(b)]. We attribute these improvements to three factors: (a) removal of NW surface passivating surfactants that inhibit carrier flow between the nanowire and metal pads, (b) removal of surfactant between adjacent NWs in the aligned assembly, and (c) interdiffusion of Au into CdSe forming an alloyed Ohmic contact, though this remains to be verified.

CONCLUSIONS

We have shown that high aspect ratio CdSe NWs with illumination-enhanced conductivity can be manipulated using microfabricated electrodes by symmetric ac DEP. The large induced dipoles of the NWs promote their self-assembly into ordered arrays. Since super-band-gap illumination generates mobile electrons and holes, thus enhancing both the conductivity and the induced dipoles in the high aspect ratio NW, a much larger DEP mobility, thus shorter assembling time than without illumination, is observed. Absorption and emission polarization anisotropy experiments show that the NW arrays exhibit a high degree of alignment. An unexpected observation is the sensitivity of the emission to applied electric fields. Specifically a factor of ~ 4 enhancements in the emission intensity is observed at low frequencies and high fields. The illumination-sensitive DEP mobility and field-enhanced fluorescent phenomena could both be attributed to a higher conductivity due to light-generated

623 mobile charges. The observed strong electric-optical field
624 coupling suggests potential uses of aligned NWs in
625 polarization-sensitive photodetection⁴² and biosensing appli-
626 cations. In this respect, earlier studies have shown that single
627 viruses can be detected through NW conductivity
628 measurements.⁴³ By the same token, the sensitivity of the
629 NW fluorescence to environment and electric fields would
630 suggest an additional means of detecting and perhaps even
631 identifying captured pathogens, enabling future improve-
632 ments in nanowire-based biosensors.

633 ACKNOWLEDGMENTS

634 Two of the authors (R.Z. and H.-C.C.) were supported
635 by a NASA Grant No. NAG3-2701 and a NSF grant. An-
636 other author (M.K.) thanks the University of Notre Dame,
637 the ACS Petroleum Research Fund, the NSF CAREER Pro-
638 gram, the Notre Dame Radiation Laboratory, and the DOE
639 Office of Basic Energy Sciences for financial support. An-
640 other author (D.J.) thanks C. Wood and Linda Chrisey C.
641 Baatar from the Office of Naval Research for valuable dis-
642 cussions. Another two authors (M.K. and D.J.) also thank the
643 Notre Dame Faculty Research Program and the Notre Dame
644 Office of Research for financial support. One of the authors
645 (M.K.) is a Cottrell Scholar of Research Corporation.

646 ¹F. Patolsky and C. M. Lieber, *Mater. Today* **20**, ■ (2005).
647 ²H. Yu, J. Li, R. A. Loomis, P. C. Gibbons, L.-W. Wang, and W. E. Buhro,
648 *J. Am. Chem. Soc.* **125**, 16168 (2003).
649 ³J. W. Grebinski, K. L. Richter, J. Zhang, T. H. Kosel, and M. Kuno, *J.*
650 *Phys. Chem. B* **108**, 9745 (2004); J. W. Grebinski, K. L. Hull, J. Zhang, T.
651 H. Kosel, and M. Kuno, *Chem. Mater.* **16**, 5260 (2004).
652 ⁴Z. A. Peng and X. G. Peng, *J. Am. Chem. Soc.* **124**, 3343 (2002).
653 ⁵A. I. Mohammad and I. P. Herman, *Appl. Phys. Lett.* **80**, 3823 (2002).
654 ⁶Y. Wu, H. Yan, M. Huang, B. Messer, J. H. Song, and P. Yang, *Chem.-Eur.*
655 *J.* **8**, 1261 (2002).
656 ⁷A. Khandelwal, D. Jena, J. W. Grebinski, K. L. Hull, and M. Kuno, *J.*
657 *Electron. Mater.* **35**, 170 (2006).
658 ⁸A. K. Singh, X. Li, A. Khandelwal, M. Kuno, H. Xing, and D. Jena
659 (unpublished).
660 ⁹V. Protasenko and M. Kuno, *Adv. Mater. (Weinheim, Ger.)* **17**, 2942
661 (2005).
662 ¹⁰M. S. Gudiksen, J. Wang, and C. M. Lieber, *J. Phys. Chem. B* **105**, 4062
663 (2001).
664 ¹¹R. Krupke, F. Hennrich, H. V. Lohneysen, and M. M. Kappes, *Science*
665 **301**, 344 (2003).

¹²A. P. Alivisatos, *J. Phys. Chem.* **100**, 13226 (1996); J. T. Hu, L. S. Li, W.
D. Yang, L. Manna, L. W. Wang, and A. P. Alivisatos, *Science* **292**, 2060
666 (2001).
667
668
669
¹³A. Shabaev and Al L. Efros, *Nano Lett.* **4**, 1821 (2004).
¹⁴I. Robel, B. Bunker, P. Kamat, and M. Kuno, *Nano Lett.* **6**, 1344 (2006).
670
671
¹⁵E. A. Muljarov, E. A. Zhukov, V. S. Dneprovskii, and Y. Masumoto, *Phys.*
Rev. B **62**, 7420 (2000).
672
673
¹⁶L.-S. Li and A. P. Alivisatos, *Phys. Rev. Lett.* **90**, 097402 (2003).
¹⁷T. Nann and J. Schneider, *Chem. Phys. Lett.* **384**, 150 (2004).
674
675
¹⁸M. E. Schmidt, S. A. Blanton, M. A. Hines, and P. Guyot-Sionnest, *J.*
Chem. Phys. **106**, 5254 (1997).
676
677
¹⁹F. Bernardini, V. Fiorentini, and D. Vanderbilt, *Phys. Rev. B* **56**, R10024
678 (1997).
²⁰P. A. Smith, C. D. Nordquist, T. N. Jackson, T. S. Mayer, B. J. Martin, J.
Mbindyo, and T. E. Mallouk, *Appl. Phys. Lett.* **77**, 1399 (2000).
679
680
²¹D. Whang, S. Jin, and C. M. Lieber, *Nano Lett.* **3**, 951 (2003); *J. Appl.*
Phys. **43**, 4465 (2004).
681
682
²²A. Tao, F. Kim, C. Hess, J. Goldberger, R. He, Y. Sun, Y. Xia, and P. Yang,
Nano Lett. **3**, 1229 (2003).
683
684
²³S. Acharya, A. B. Panda, N. Belman, S. Efrima, and Y. Golan, *Adv. Mater.*
(Weinheim, Ger.) **18**, 210 (2006).
685
686
²⁴R. Zhou, P. Wang, and H.-C. Chang, *Electrophoresis* **27**, 1376 (2006).
687
²⁵Y. Huang, X. Duan, Q. Wei, and C. M. Lieber, *Science* **291**, 630 (2001).
688
²⁶K. Yamamoto, S. Akita, and Y. Nakayama, *J. Phys. D* **31**, L31 (1998).
689
²⁷R. Krupke, F. Hennrich, H. Lohneysen, and M. Kappes, *Science* **301**, 344
690 (2003).
691
²⁸M. Dimaki and P. Boggild, *Phys. Status Solidi A* **203**, 1088 (2006).
692
²⁹E. Rothenberg, M. Kazes, E. Shaviv, and U. Banin, *Nano Lett.* **5**, 1581
693 (2005).
694
³⁰J. J. Boote and S. D. Evans, *Nanotechnology* **9**, 1500 (2005).
695
³¹K. L. Hull, J. W. Grebinski, T. H. Kosel, and M. Kuno, *Chem. Mater.* **17**,
4416 (2005).
696
697
³²J. Wu, Y. Ben, D. Battigelli, and H.-C. Chang, *Ind. Eng. Chem. Res.* **44**,
2815 (2005).
698
699
³³H. A. Pohl, *Dielectrophoresis* (Cambridge University Press, Cambridge,
1978).
700
³⁴M. Kuno, O. Ahmad, V. Protasenko, D. Bacinello, and T. Kosel, *Chem.*
Mater. **18**, 5722 (2006).
701
702
³⁵*Semiconductors: Other than Group IV Elements and III-V Compounds*,
edited by O. Madelung (Springer, New York, 1992), p. 29.
703
704
³⁶Z. Gagnon and H.-C. Chang, *Electrophoresis* **26**, 3725 (2005).
705
706
³⁷P. V. Kamat et al., *J. Am. Chem. Soc.* **126**, 10757 (2004).
707
³⁸X. Q. Chen and T. Saito, *Appl. Phys. Lett.* **78**, 3714 (2001).
708
709
³⁹C. R. Kagan, C. B. Murray, and M. G. Bawendi, *Phys. Rev. B* **54**, 8633
710 (1996).
⁴⁰M. Kuno (private communication).
711
712
⁴¹S. A. Empedocles and M. G. Bawendi, *Science* **278**, 2114 (1997).
⁴²A. Singh, A. Khandelwal, X. Li, H. Xing, M. Kuno, and D. Jena, *Digest of*
Device Research Conference, Pennsylvania State University, PA, June
2006 (unpublished).
713
714
715
⁴³F. Patolsky, G. Zheng, O. Hayden, M. Lakadamyali, X. Zhuang, and C. M.
Lieber, *Proc. Natl. Acad. Sci. U.S.A.* **101**, 14017 (2004).
716
717

AQ:
#8AQ:
#9AQ:
#10AQ:
#11AQ:
#12

AUTHOR QUERIES — 066706JAP

- #1 Au: JAP DOES NOT ALLOW CLAIMS OF NOVELTY. PLEASE CHECK DELETION OF “new” THROUGHOUT.
- #2 Au: REF. 24 WAS CITED PREMATURELY. PLEASE CHECK.
- #3 Au: REF. 29 WAS NOT CITED IN TEXT. PLEASE CHECK OUR INSERTION.
- #4 Au: REFERENCES MUST BE CITED IN ORDER. PLEASE CHECK OUR RENUMBERING.
- #5 Au: “cp” WAS CHANGED TO “cP” (centipoised). PLEASE CHECK.
- #6 Au: PLEASE CHECK CHANGES IN “K is the complex...”
- #7 Au: PLEASE CHECK CITATIONS OF FIGS. 9(a) AND 9(b) IN TEXT. THERE ARE ONLY EIGHT FIGURES.
- #8 Au: PLEASE CHECK CHANGES IN THE ACKNOWLEDGMENTS.
- #9 Au: PLEASE UPDATE REF. 8.
- #10 Au: PLEASE SUPPLY ALL AUTHORS IN REF. 37 IF FEWER THAN NINE
- #11 Au: PLEASE UPDATE REF. 40.
- #12 Au: PLEASE UPDATE REF. 42

PROOF COPY 066706JAP